Continuously Infusing Hyperpolarized ^{129}Xe into Flowing Aqueous Solutions Using Hydrophobic Gas Exchange Membranes

Zackary I. Cleveland,[†] Harald E. Möller,[†,‡] Laurence W. Hedlund,[†] and Bastiaan Driehuys*[,†]

Center for In Vivo Microscopy, Duke University Medical Center, Durham, NC, and Max Planck Institute for Human Cognitive and Brain Sciences, Leipzig, Germany

Received: May 27, 2009; Revised Manuscript Received: July 27, 2009

Hyperpolarized (HP) ^{129}Xe yields high signal intensities in nuclear magnetic resonance (NMR) and, through its large chemical shift range of ~300 ppm, provides detailed information about the local chemical environment. To exploit these properties in aqueous solutions and living tissues requires the development of methods for efficiently dissolving HP ^{129}Xe over an extended time period. To this end, we have used commercially available gas exchange modules to continuously infuse concentrated HP ^{129}Xe into flowing liquids, including rat whole blood, for periods as long as one hour and have demonstrated the feasibility of dissolved-phase MR imaging with submillimeter resolution within minutes. These modules, which exchange gases using hydrophobic microporous polymer membranes, are compatible with a variety of liquids and are suitable for infusing HP ^{129}Xe into the bloodstream in vivo. Additionally, we have developed a detailed mathematical model of the infused HP ^{129}Xe signal dynamics that should be useful in designing improved infusion systems that yield even higher dissolved HP ^{129}Xe signal intensities.

1. Introduction

Gas-phase ^{129}Xe is increasingly used in a variety of disciplines because of this isotope's unique magnetic resonance (MR) characteristics.[1,2] Through its large chemical shift range of ~300 ppm, pronounced chemical shift anisotropy (CSA),[3,4] and variable longitudinal relaxation,[5−7] ^{129}Xe provides a wealth of information about its chemical environment. Additionally, the nuclear spin polarization of ^{129}Xe can be enhanced by orders of magnitude using spin exchange optical pumping (SEOP),[8] enabling novel MR applications such as probing single crystal surfaces,[9] measuring the permeability and tortuosity of porous materials,[10,11] and examining combustion processes.[12] Hyperpolarized (HP) ^{129}Xe also permits magnetic resonance imaging (MRI) of structure and gas exchange pathways in both healthy and injured lungs,[13−15] which makes this isotope of biomedical interest. However, the greatest promise for ^{129}Xe in biomedicine stems from its reasonably high solubility (~10%) in aqueous solutions and tissues.[16]

In solution, ^{129}Xe can be used to probe protein structure[17−19] and physiologically important parameters such as blood oxygenation.[20] Dissolved HP ^{129}Xe residing in the pulmonary capillaries rapidly diffuses into the alveolar gas spaces where its resonance frequency is shifted by ~200 ppm. Thus, HP ^{129}Xe can serve as a spatially resolved probe of pulmonary function.[21] Dissolved HP ^{129}Xe also allows MR studies to extend beyond the lungs to organs including the brain,[22] where multiple ^{129}Xe resonances are observed.[23] Additionally, HP ^{129}Xe MR, when used in concert with xenon encapsulating cryptophane biosensors,[24] allows the sensitive detection of proteins[25,26] and nucleic acids[27] and shows promise as molecular imaging contrast agent.[28] Despite this range of applications, aqueous HP ^{129}Xe studies are relatively infrequent.

This low number of solution studies results in part from the difficulties involved in efficiently dissolving HP ^{129}Xe at high concentrations. Typically, HP ^{129}Xe is dissolved by introducing gaseous xenon into a container above the solution of interest and then manually shaking the container.[29,30] This method requires that the solutions be degassed before experiments to prevent longitudinal relaxation through dipole coupling to paramagnetic O_2 gas. However, degassing introduces considerable experimental delays and the approach is limited to solutions that are not damaged by evacuation or freeze−thaw cycles. For more fragile systems, such as blood,[20,31,32] the HP ^{129}Xe-saturated solution must be prepared separately and then delivered, usually by injection, into the sample of interest. This subsequent injection avoids depolarization by oxygen and degassing-induced mechanical damage but, at least to some degree, alters the chemical composition of the sample.

Alternately, HP ^{129}Xe can be dissolved by flowing gas from the polarizer and bubbling the SEOP mixture directly into the solution of interest.[33] Bubbling enables signal averaging by providing continuous HP ^{129}Xe signal and can be applied to flowing solutions. However, bubbling yields low dissolved xenon concentrations due to the low xenon partial pressures typically used in SEOP (~1% xenon)[34] and can lead to susceptibility artifacts unless liquid flow is stopped during data acquisition.[35] Further, this method is limited to in vitro studies because, if attempted in vivo, xenon bubbles could produce fatal gas emboli.

Recently, Baumer et al.[36] produced high dissolved HP ^{129}Xe signal intensities by passing HP gas through hollow, microporous polymer membrane fibers. The hydrophobicity of these hollow membrane fibers prevented fluids from wetting the interior of the fibers and membrane pores, allowing HP ^{129}Xe to continuously diffuse through the pores directly into the sample. However, directly infusing into the solution within the detection region allows gas-phase HP ^{129}Xe to be subjected to

* To whom correspondence should be addressed. Address: Center for In Vivo Microscopy, Department of Radiology, Box 3302, Duke University Medical Center, Durham, NC 27710. Telephone: (919) 684-7786. Fax: (919) 684-7158. E-mail: bastiaan.driehuys@duke.edu.

[†] Duke University Medical Center.

[‡] Max Planck Institute for Human Cognitive and Brain Sciences.

10.1021/jp9049582 CCC: $40.75
Published on Web 08/24/2009

RF excitation. In experiments where chemical shift selective pulses cannot be used, gas-phase HP ^{129}Xe will inevitably be excited, depolarizing the longitudinal gas-phase magnetization and producing transverse gas-phase magnetization that could diffuse into solution and interfere with phase dependent and T_2 dependent experiments.

In this work, we describe the use of commercially available gas exchange modules to infuse HP ^{129}Xe into flowing solutions outside the RF coil. Because infusion occurs remotely, hard RF pulses can be used without exciting and depolarizing the gas-phase magnetization. Further, this method requires no special sample pretreatment and operates at near ambient pressure with fully concentrated HP ^{129}Xe. Compared to dilute SEOP mixtures, it produces higher dissolved HP ^{129}Xe concentrations and thus improved signal intensities. The large signals enable dissolved-phase HP ^{129}Xe imaging with submillimeter resolution with total acquisition times of a few minutes. Moreover, continuous infusion enables nonequilibrium signal to be detected for up to an hour using only 300 mL of xenon gas at ambient pressure and temperature.

Finally, we describe the infused HP ^{129}Xe signal dynamics with a detailed mathematical model that incorporates the effects of gas and fluid flow, mass transport across the exchange membranes, and ^{129}Xe longitudinal relaxation. This model elucidates a number of important features of the infused HP ^{129}Xe signal dynamics and can, therefore, be used to guide the development of improved HP ^{129}Xe infusion systems.

2. Experimental Methods

2.1. Method Overview. Within a gas exchange module (see Figure 1A), gaseous HP ^{129}Xe does not immediately contact the liquid, but rather diffuses through 0.04 μm pores within a bundle of hollow polypropylene membrane fibers (Celgard X50, Membrana, Charlotte, NC). The volume within the module that is accessible to the liquid is known as the "empty volume" and was 2.7 mL for the modules used in this work. Because the membrane fibers are highly hydrophobic, liquids within the module empty volume cannot wet the microscopic membrane pores and are thus prevented from reaching the interior of membrane fibers. In contrast, gases such as HP ^{129}Xe located within the hollow fibers can continuously diffuse through the membrane pores into solution.

Although these membranes enable rapid gas dissolution, the final dissolved gas concentration cannot exceed the limit set by the Ostwald solubility of the gas. For gases with solubilities that are less than one, such as the xenon, nitrogen, and helium used in this work, the concentration of the gas within the hollow fibers will always be greater than the concentration in solution. Provided that there is a constant supply of gas, the mass transport across the membrane is therefore expected to be essentially independent of gas flow.[37] However, slow gas flows would lead to extended HP ^{129}Xe residence times within the gas transfer tubing and the hollow membrane fibers and cause unacceptable levels of gas-phase longitudinal relaxation. To limit polarization losses, all of the experiments involving membranes described in this work were performed by flowing excess HP ^{129}Xe gas through the module. HP ^{129}Xe that was not dissolved by the flowing aqueous solution is referred to throughout the text as "exhaust".

Unless otherwise stated, the excess xenon mixtures were exhausted to outside the superconducting magnet through an unrestricted polyethylene tube. The exhaust gas could thus freely pass through the exchange module without producing gas bubbles in the liquid as long as the pressure on the liquid side

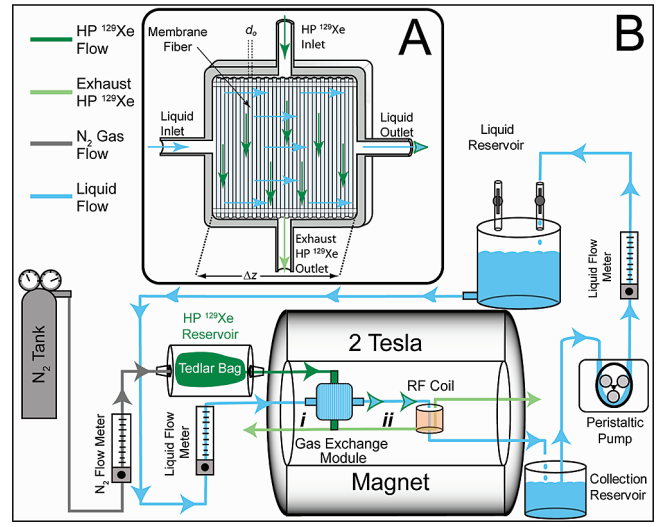

Figure 1. Schematic depicting HP ^{129}Xe infusion. (A) Gas exchange module. HP ^{129}Xe enters the module and flows through a bundle of hollow, hydrophobic membrane fibers, having an outer diameter of d_o. The fibers are perforated with submicrometer pores, but the hydrophobicity of the fibers prevents the liquid from wetting the interior of membranes. Thus, gas freely diffuses out of the hollow fibers and into solution. Undissolved gas passes as exhaust to the exterior of the module. Liquid enters the module and flows a distance of Δz around the outside of the hollow fibers. The volume within the module not occupied by the fibers is accessible to the liquid and referred to as the empty volume. (B) Experimental setup. HP ^{129}Xe flows from a Tedlar bag located within a pressurized cylinder into the exchange module. Excess HP ^{129}Xe gas could (*i*) be exhausted outside the magnet or (*ii*) be passed through the RF coil to provide a gas-phase reference. Liquid passes from an elevated reservoir, through a direct reading flow meter, and then through the module. After passing through an RF coil, the liquid is collected in a second reservoir and returned to the supply reservoir using a peristaltic pump.

of the membranes exceeded the gas pressure within the fibers. This requirement for bubble-free gas infusion for both the pure xenon and the xenon, nitrogen, and helium containing SEOP gas mixture was met in all of the experiments described in this work.

2.2. ^{129}Xe Polarization. Either natural abundance (26% ^{129}Xe, Airgas National Welders Inc., Durham, NC) or isotopically enriched (83% ^{129}Xe, Spectra Gases Inc., Alpha, NJ) xenon was hyperpolarized by SEOP[8,38] using a prototype commercial polarizer (model 9800, MITI, Durham, NC). This system employs a continuous flow of dilute xenon (1% xenon, 89% helium, and 10% N_2) passing through a rubidium vapor-containing optical cell at 160 °C and a pressure of 5 atm. After exiting the cell, HP ^{129}Xe can be cryogenically extracted from the buffer gases using liquid nitrogen[34] with final polarizations of 5−10%. In other experiments, the dilute HP ^{129}Xe mixture was allowed to flow from the polarizer at ∼150 mL/min without cryogenic extraction.[39] In this method, SEOP was also performed at 5 atm but was passed through a perfluoroalkoxy polymer (PFA) regulator (Partek, Tuscon, AZ) to reduce the total gas pressure to ∼1 atm.

2.3. Membrane Infusion of HP ^{129}Xe. Following cryogenic accumulation, xenon ice was removed from liquid nitrogen and thawed into 350 ml Tedlar bags (Jensen Inert Products, Coral Springs, FL) located within a Plexiglas cylinder. The cylinder was immediately placed within the fringe field of the superconducting magnet and aligned with the bore of the magnet to minimize relaxation due to transverse magnetic field gradients.[40] The bag was then pressurized to ∼1.2 kPa above ambient pressure by flowing N_2 gas from a supply tank into the cylinder (see Figure 1B). The flow of xenon out of the bag was initiated

by opening a plastic stopcock and was controlled using a direct reading gas flow meter (Cole-Parmer, Vernon Hills, IL) located inline between the xenon containing cylinder and the N_2 supply tank.

Because of the small applied N_2 pressure, the gas volume that entered the reservoir and compressed the collapsing Tedlar bag was essentially identical to the HP ^{129}Xe volume that flowed from the bag toward the exchange module. By controlling the N_2 flow into the Tedlar bag reservoir, the xenon flow could be controlled without passing the gas through potentially depolarizing flow constrictors. After traversing ~1.2 m of polyethylene tubing [outer diameter (OD) = 3.2 mm, inner diameter (ID) = 1.6 mm], HP ^{129}Xe was infused directly into aqueous solution using a Liqui-Cel MicroModule (Membrana, Charlotte, NC) located within the magnet bore.

Unless otherwise stated, the liquid flowed from a 5 L polyethylene reservoir (Nalgene, Thermo Fisher Scientific Inc., Waltham, MA) located 2.4 m above the magnet bore (Figure 1B). Liquid flow was controlled by a direct-reading water flow meter (Cole-Parmer) located between the liquid reservoir and the exchange module. After passing through the module, liquid was collected in a second polyethylene reservoir (Nalgene) and returned to the supply reservoir using a peristaltic pump (MasterFlex, Cole-Parmer). Return flow was monitored by a direct-reading flow meter (Cole-Parmer) between the pump and the supply reservoir and was maintained at the same flow as the liquid exiting the supply reservoir. Alternatively, a peristaltic pump alone was used to continuously recirculate ~5 mL of liquid in a closed circuit.

2.4. HP ^{129}Xe MR Imaging and Spectroscopy. Images and spectra were acquired using a 2.0 T, 30 cm bore, horizontal superconducting magnet (Oxford Instruments, Oxford, UK) with shielded gradients (400 mT/m), controlled by a GE EXCITE 12.0 console (GE Healthcare, Milwaukee, WI). The scanner was interfaced with 23.66 MHz linear RF coils by an integrated transmit/receive switch with 31 dB gain preamplifier (Nova Medical, Wilmington, MA) and made to operate at 23.66 MHz instead of its intrinsic 63.86-MHz frequency using an up−down converter (Cummings Electronics Laboratories, North Andover, MA). Dissolved ^{129}Xe images were obtained with isotopically enriched xenon using an 8 cm long, 7 cm diameter birdcage coil. The images were obtained from a phantom comprising a 15 cm long, 1.6 mm ID polyethylene tube coiled around a 4 cm long, 1.5 cm OD cylinder and were acquired using a nonslice-selective gradient-echo sequence with a 30° flip angle, repetition time (TR) = 500 ms, bandwidth = 4 kHz, matrix = 64 × 64, field of view (FOV) = 4.0 cm, and number of acquisitions = 16. HP ^{129}Xe spectra were obtained from natural abundance xenon using the probe described above or a 6.6 cm long, 3.3 cm diameter solenoid probe.

To obtain flow-dependent relaxation data, concentrated HP ^{129}Xe at a fixed gas flow was infused into distilled water or aqueous 0.02 M $CuSO_4$ at liquid flows of 4−50 mL/min. Prior to RF excitation, the liquid flow was halted using a plastic stopcock located immediately outside the RF coil. To measure relaxation in fully degassed samples, cryogenically accumulated HP ^{129}Xe was dispensed into a 100 mL Pyrex shaker[30] containing 30−40 mL distilled water that had been degassed by evacuation with a rotary vane vacuum pump (Pfeiffer Vacuum, Nashua, NH). The shaker was then moved to the 0.2 T fringe field of the MR imaging magnet, where it was shaken vigorously by hand for 20 s to dissolve the ^{129}Xe gas. HP ^{129}Xe saturated solution was then withdrawn into a 10 mL plastic syringe and immediately placed in the RF coil.

T_1 measurements were performed by observing the dissolved HP ^{129}Xe magnetization with a series of small evenly spaced RF pulses. For distilled water 32, 1° pulses were applied. To compensate for the lower ^{129}Xe polarization in the 0.02 M $CuSO_4$ solution, 16, 5° RF pulses were used. The data were fit to monoexponential decays with corrections applied for magnetization lost to the RF pulses.

Spectra were processed using HiRes Version 1.6 (Hatch Center for MR Research, Columbia University, New York, NY). Data fitting was performed in Igor Pro (Wavemetrics, Inc., Lake Oswego, OR) or routines written in MATLAB (The MathWorks, Inc., Natick, MA). Simulations were also performed using MATLAB.

2.5. Animal Care and Use. Blood was taken from a 645 g, male Sprague-Dawley rat (Charles River, Raleigh, NC) following a protocol approved by the Duke University Institutional Animal Care and Use Committee. Briefly, the rat was anesthetized with intraperitoneal (IP) injection of 65 mg/kg Nembutal (sodium pentobarbital) and heparinized (420 UI/kg) before withdrawing 15 mL of blood from the carotid artery. The animal was then euthanized by an overdose of pentobarbital.

3. Mathematical Model

3.1. Mass Transfer. To make the fullest use of membrane-based HP ^{129}Xe infusion, it will be necessary to quantitatively understand the factors that govern magnetization transport from the gas-phase into solution. Because these membranes are of considerable practical interest due to their common use in extracorporeal blood oxygenation,[41] their mass transport properties have been extensively studied and characterized.[37,42] By adapting the results of these earlier studies and including the influence of longitudinal relaxation, we have developed a detailed model describing the observable HP ^{129}Xe magnetization obtained using gas exchange membranes.

The mass transfer of a substance from the gas-phase into a liquid across a bundle of hollow fiber gas-exchange membranes with total surface area, A_m, can be described in analogy to Fick's law by[43]

$$\frac{1}{A_m}\frac{dn}{dt} = K(c_{l,eq} - c_l) \tag{1}$$

where n and c_l are the number of moles and the concentration of the solute gas, respectively; $c_{l,eq}$ is the concentration in the liquid that would be in equilibrium with the gas phase; t is time; and K is the mass-transfer coefficient (units m/s). Assuming that the liquid flow through the gas-exchange module is along the z-direction and characterized by a flow rate, Q_l, eq 1 can be rewritten as

$$\frac{1}{A_m}\frac{dn}{dt} = \frac{V_l}{A_m}\frac{dc_l}{dt} = \frac{uV_l}{A_m}\frac{dc_l}{dz} = \frac{Q_l\Delta z}{A_m}\frac{dc_l}{dz} = K(L_l c_g - c_l) \tag{2}$$

where V_l is the module empty volume (liquid volume within the module); Δz is the length of the module in the direction of liquid flow; and $u = \Delta z Q_l/V_l$ is the liquid velocity. Note that $c_{l,eq}$ has now been expressed in terms of the gas-phase concentration, c_g, by employing the definition of the Ostwald solubility (i.e., $L_l = c_{l,eq}/c_g$). Integrating eq 2 with respect to c_l on the interval from the concentration at the module inlet, c_{in}, to the concentration at the module outlet, c_{out}, and solving for c_{out} yields

$$c_{out} = L_l c_g + (c_{in} - L_l c_g)\exp\left(K\frac{A_m}{Q_l}\right) \quad (3)$$

For hollow-fiber gas-exchange membranes, the mass-transfer coefficient used in eqs 1−3 is most conveniently expressed as[37,43]

$$K = \frac{\mathrm{Sh}D_l}{d_e} \quad (4)$$

where Sh is the dimensionless Sherwood number; D_l is the diffusion coefficient of the dissolved solute; and d_e is the equivalent diameter of the flow path, defined by[42,44]

$$d_e = \frac{\varepsilon}{1-\varepsilon}d_0 \quad (5)$$

In eq 5, ε is the void fraction of the gas-exchange module, which is defined as the ratio of the module empty volume, V_l, to the total volume of the module, V_{tot}; d_0 is the outside diameter of the hollow fibers. The Sherwood number in turn can be expressed in terms of the mass-transfer correlation by

$$\mathrm{Sh} = a\mathrm{Re}^b\mathrm{Sc}^c \quad (6)$$

where a, b, and c are empirical constants.[42] In eq 6, Re and Sc are the Reynolds and Schmidt numbers given by

$$\mathrm{Re} = \frac{ud_e\rho}{\eta} \quad (7)$$

and

$$\mathrm{Sc} = \frac{\eta}{\rho D_l} \quad (8)$$

where, η and ρ are the dynamic viscosity and density of the liquid, respectively. Note that the expression for d_e given in eq 5, and thus the definition of Re in eq 7, is strictly valid only for fully developed turbulent flow.[42,45] However, both expressions are used extensively in modeling hollow fiber membrane blood oxygenators and lead to predicted mass transfer behavior that agrees well with experimental observations.[37,42]

Combining eqs 4−8 allows the mass transfer coefficient to be expressed as

$$K = ad_e^{b-1}D_l^{1-c}\left(\frac{\Delta z Q_l}{V_l}\right)^b\left(\frac{\rho}{\eta}\right)^{b-c} \quad (9)$$

Together, eqs 5 and 9 permit the mass transfer coefficient to be calculated for a given set of experimental conditions using only the physical properties of the fluid, the fiber and module dimensions, and experimentally determined values that can be obtained from the literature. These values, along with the relevant references, are provided in Table 1.

3.2. Polarization Transfer. While the ability to calculate the mass transport of xenon and thus the xenon concentration in solution is a necessary step in quantifying the signal dynamics of infused HP ^{129}Xe, additional factors must be taken into account to reflect that in MR, we are not primarily concerned with concentration but rather magnetization. The dissolved longitudinal magnetization, $m_{z,l}$, may be expressed as

$$m_{z,l} = \frac{1}{2}c_l N_A|\gamma|\hbar P_l \quad (10)$$

where N_A is Avogadro's constant; γ is the gyromagnetic ratio of the nucleus; $\hbar$ is Planck's constant divided by 2π; and P_l is the nuclear polarization of the solute. By differentiating eq 10, the rate of the change in magnetization can be expressed as

$$\frac{dm_{z,l}}{dt} = \frac{1}{2}N_A|\gamma|\hbar\left(P_l\frac{dc_l}{dt} + c_l\frac{dP_l}{dt}\right) \quad (11)$$

where the change in solute concentration is given by eq 1. Neglecting the small contribution from thermal polarization, the change in dissolved polarization can be approximated by a first-order decay with time constant, $T_{1,l}$. Thus, eq 11 becomes

$$\frac{dm_{z,l}}{dt} = K\frac{A_m}{V_l}(Lm_{z,i} - m_{z,l}) - \frac{1}{T_{1,l}}m_{z,l} \quad (12)$$

where $m_{z,i}$ is the gas-phase magnetization at the gas−liquid interface.

For the setup depicted in Figure 1B, it may be assumed that the liquid enters the module at time $t = 0$ with no initial magnetization and exits after a residence time, $\Delta t = V_l/Q_l$. Integrating eq 12 according to

$$\int_0^\tau dt = \int_0^{m_{z,out}} \frac{dm_{z,l}}{K\frac{A_m}{V_l}L_l m_{z,i} - \left(K\frac{A_m}{V_l} + \frac{1}{T_{1,l}}\right)m_{z,l}} \quad (13)$$

leads to a magnetization at the liquid outlet, $m_{z,out}$, of

$$m_{z,out} = L_l\frac{K\frac{A_m}{V_l}}{K\frac{A_m}{V_l} + \frac{1}{T_{1,l}}}m_{z,i}\left\{1 - \exp\left[-\left(K\frac{A_m}{V_l} + \frac{1}{T_{1,l}}\right)\frac{V_l}{Q_l}\right]\right\} \quad (14)$$

Finally, the dissolved ^{129}Xe magnetization at the module outlet will be decreased by longitudinal relaxation during transport to the detection region. The magnetization that will be observed after transport, $m_{z,obs}$, will thus be given by

$$m_{z,obs} = m_{z,out}\exp\left(\frac{-\tau_l}{T_{1,l}}\right) \quad (15)$$

where $\tau_l = V_{l,t}/Q_l$ is the liquid transit time through the transfer line with volume, $V_{l,t}$. From the above discussion, in particular

TABLE 1: Nonstandard Symbols and Literature Values Used in the Mathematical Model

symbol	meaning	value	ref.
a, b, c	empirical constants	$a = 0.8$, $b = 0.59$, $c = 0.33$	42
B_{O_2}	relaxivity of O_2 gas	8.7×10^{-3} m^3 mol^{-1} s^{-1}	49
A_m	gas-exchange surface area of the module	0.01 m^2	[a]
A_p	surface area of a membrane pore	$2\pi rl$	
c_g	gas-phase concentration		
c_l	solute concentration in the liquid		
$c_{l,eq}$	equilibrium solute concentration		
c_{in}	solute concentration at the module inlet		
$c_{O_2,atm}$	concentration of O_2 gas in the atmosphere	8.6×10^{-3} mol L^{-1}[b]	
c_{out}	solute concentration at the module outlet		
d_e	equivalent diameter	eq 5	
d_o	outer diameter of the membrane fibers	3×10^{-4} m	[a]
D_d	xenon diffusion coefficient in the polymer	3.8×10^{-12} m^2 s^{-1}	54
D_g	gas-phase xenon diffusion coefficient	5.71×10^{-6} m^2 s^{-1}[c]	55
D_l	diffusion constant of dissolved xenon	$2.2 \pm 0.4 \times 10^{-9}$ m^2 s^{-1}[d]	56
ε	void fraction of the gas-exchange module	$V_l/(V_l + V_f)$	
K	mass transport coefficient	eq 9	
l	length of the pore (membrane thickness)	4×10^{-5} m[e]	[a]
L_l	Ostwald solubility of xenon in water	0.1068[d]	16
L_{O_2}	Ostwald solubility of O_2 in water	0.027[d]	57
L_p	Ostwald solubility of xenon in polypropylene	0.682 ± 0.03	47
$m_{z,gas}$	^{129}Xe magnetization entering the module		
$m_{z,i}$	^{129}Xe magnetization at the gas−liquid interface		
$m_{z,l}$	dissolved ^{129}Xe magnetization		
$m_{z,out}$	dissolved ^{129}Xe magnetization in the liquid leaving the module		
$m_{z,obs}$	observable ^{129}Xe magnetization in the liquid		
n	number of moles of xenon in solution		
η	dynamic viscosity of water	8.90×10^{-4} Pa s[d]	58
P_l	nuclear polarization of ^{129}Xe in solution		
Q_g	gas flow		
Q_l	liquid flow		
r	membrane pore radius	2×10^{-8} m[f]	[a]
ρ	liquid density (water)	997 kg m^{-3}[c]	58
Re	Reynolds number	eq 7	
Sc	Schmidt number	eq 8	
Sh	Sherwood number	eq 6	
S	infused HP ^{129}Xe signal intensity		
τ_f	xenon gas transit time through the fibers	$\tau_f = V_f/2Q_g$	
τ_l	liquid transit time from the exchange module to the detection region	$\tau_l = V_{l,t}/Q_l$	
τ_p	xenon transit time through the membrane pores	$\tau_p = l^2/2D_g$	
$T_{1,d}$	^{129}Xe longitudinal relaxation time in polymer	7.6 ± 0.3 to 8.1 ± 0.4 s[g]	59
$T_{1,f}$	^{129}Xe longitudinal relaxation time in the hollow membrane fibers		
$T_{1,l}$	^{129}Xe longitudinal relaxation time in the liquid		
$T_{1,p}$	^{129}Xe longitudinal relaxation time in the membrane pore		
u	liquid velocity within the module	$\Delta z Q_l/V_l$	
V_f	total volume of hollow fibers	$A_m d_o/4$	
V_l	empty volume (liquid volume in the module)	2.7×10^{-6} m^3	
$V_{l,t}$	transfer line volume	2.26×10^{-6} m^3[h]	
V_p	volume of a membrane pore	$\pi r^2 l$	
V_{tot}	total volume of the exchange module	$V_l + V_f$	
z	cartesian coordinate in the direction of liquid flow within the module		
Δz	module length in the direction of liquid flow	0.020 m	[a]

[a] From Membrana/Celgard technical literature. [b] Assuming the ambient air is 21% O_2 at 1 atm and 25 °C. [c] For pure xenon gas at 1 atm. [d] In water at 25 °C. [e] The nominal membrane thickness stated by the manufacturer. [f] Half of the nominal pore size stated by the manufacturer. [g] Reference 59 did not state whether the polymer used in the study was polypropylene or polyethylene. However, in both polymers the longitudinal relaxation is expected to be dominated by dipolar coupling to protons,[6] and the ^{129}Xe T_1 values should therefore be similar for either polymer. [h] For the experimental setup used with the distilled water and the 0.02 M $CuSO_4$. For the blood sample, the value was 1.0 mL.

eqs 14 and 15, the signal intensity, S, observed from infused HP ^{129}Xe can be expressed as

$$S = \kappa_P \cdot L_l \frac{K\frac{A_m}{V_l}}{K\frac{A_m}{V_l} + \frac{1}{T_{1,l}}}\left\{1 - \exp\left[-\left(K\frac{A_m}{V_l} + \frac{1}{T_{1,l}}\right)\frac{V_l}{Q_l}\right]\right\} \times \exp\left(\frac{-V_{l,t}}{T_{1,l}Q_l}\right) \quad (16)$$

where κ_P is a proportionality constant that accounts for factors such as the coil sensitivity and the polarization of HP ^{129}Xe at the gas−liquid interface within the module.

3.3. Gas-phase HP ^{129}Xe Longitudinal Relaxation. To fully describe how experimental parameters influence the signal intensity obtained from infused HP ^{129}Xe, gas-phase polarization losses prior to dissolution must also be considered. Thus, in addition to the factors listed in eqs 14 and 15, we will have

$$m_{z,i} = m_{z,g}\exp\left(\frac{-\tau_p}{T_{1,p}}\right)\exp\left(\frac{-\tau_f}{T_{1,f}}\right) \quad (17)$$

where $m_{z,g}$ is the initial gas-phase ^{129}Xe magnetization entering the exchange module; τ_p is the xenon gas transit time through the membrane pores; τ_f is the xenon transit time through the hollow-fibers; and $T_{1,p}$ and $T_{1,f}$ are the gas-phase spin−lattice

relation times in the membrane pores and the hollow fibers, respectively.

We assume that xenon transport across the membrane is driven simply by one-dimensional diffusion through the pores. This assumption is reasonable because mass transport driven by pressure gradients would produce bubbles on the liquid side of membrane, which were not observed in the experimental work. Hence, transit time through the membrane pores is given by $\tau_p = l^2/2D_g$, where l is the length of the pore and D_g is the gas-phase diffusion coefficient of xenon.

The purely gas-phase longitudinal relaxation time for ^{129}Xe in pure xenon gas will exceed 4 h at pressures near 1 atm[46] and can be considered negligible. Therefore, the relaxation in pure xenon is expected to be dominated by dissolution into the polymer, and the relaxation rate will be given by[47,48]

$$\frac{1}{T_{1,p}} = L_p\left(\frac{A_p}{V_p}\right)\sqrt{\frac{D_d}{T_{1,d}}} \tag{18}$$

where L_p is the Ostwald solubility of xenon in the polymer; A_p is the surface area of the pore; V_p is the volume of the pore; D_d is the diffusion coefficient of xenon dissolved in the polymer; and $T_{1,d}$ is the relaxation time of ^{129}Xe dissolved in the polymer. By assuming that the pores are cylinders of radius, r, eqs 17−18 yield

$$\exp\left(\frac{-\tau_p}{T_{1,p}}\right) = \exp\left(\frac{-l^2 L_p}{D_g r}\sqrt{\frac{D_d}{T_{1,d}}}\right) \tag{19}$$

Inserting the values from Table 1 into eq 19, with $T_{1,d} = 7.6$ s, yields $\exp(-\tau_p/T_{1,p}) \approx 0.99$. This expectation of negligible polarization loss due to relaxation within the membrane pores is in agreement with the empirical results of Baumer et al.[36] Note that even if relaxation caused by the presence of O_2 gas is considered (see the discussion that follows), the relaxation within the pores is still negligible because of the short time required for xenon gas to diffuse a distance of $l = 40$ μm. Similarly, the relaxation rate due to dissolution into the fibers can be expressed as

$$\frac{1}{T_{1,f}} = L_p\left(\frac{A_m}{V_f}\right)\sqrt{\frac{D_d}{T_{1,d}}} \tag{20}$$

where V_f is the gas volume of the fibers. (Note that for simplicity, we ignore the small volume occupied by the membranes themselves).

While eq 20 accounts for relaxation due to dissolution into the hollow fiber membranes, O_2 within the gas space of the fibers may contribute to polarization loss. The highest O_2 gas concentration, and thus the maximum ^{129}Xe relaxation rate, will occur if water enters the module at equilibrium with the atmosphere and then equilibrates with the initially O_2-free gas space within the fibers. Under these conditions, the relaxation rate within the fibers would be given by

$$\frac{1}{T_{1,f}} = L_p\left(\frac{A_m}{V_f}\right)\sqrt{\frac{D_d}{T_{1,d}}} + B_{O_2}\frac{L_{O_2}c_{O_2,atm}V_l}{L_{O_2}V_l + V_f} \tag{21}$$

where B_{O_2} is the relaxivity of O_2 gas,[49] L_{O_2} is the Ostwald solubility of O_2 in water, and $c_{O_2,atm}$ is the atmospheric O_2 concentration. Unlike the xenon in membrane pores, mass transport through the hollow fibers will be dominated by gas flow, Q_g, rather than diffusion. Because HP ^{129}Xe can diffuse through the membrane at any point along the length of the fiber, it is appropriate to calculate the relaxation using the average residence time of $\tau_f = V_f/2Q_g$.

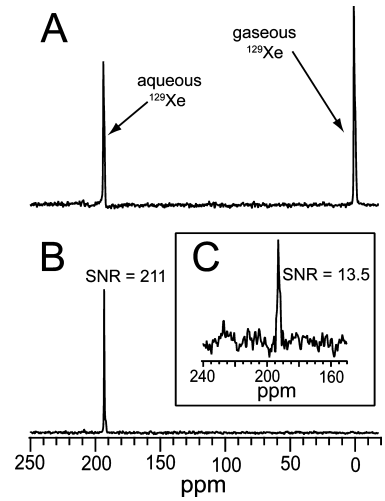

Figure 2. Spectra from HP ^{129}Xe infused into distilled water. All spectra were acquired with a 5 kHz bandwidth and are referenced to the gas-phase peak at 0 ppm. Ten Hz broadening were applied. (A) Spectrum obtained from a hard 90° RF pulse with liquid and gas flows of 20 mL/min and 5 mL/min, respectively. A gas-phase peak is observed because xenon exhausted from the exchange module was passed through the RF coil. (B) Aqueous HP ^{129}Xe spectrum obtained under the same conditions as in panel A except that the excess was exhausted outside the magnet. (C) Spectrum obtained from dilute HP ^{129}Xe (1% xenon) flowing from the xenon polarizer through the exchange module by averaging 312, 90° RF pulses (TR = 5 s). The water and gas flows were 20 mL/min and 150 mL/min, respectively.

From the above discussion, it is now possible to express the observable magnetization as a function of both liquid flow and gas flow as

$$m_{z,obs} = \frac{L_l m_{z,g}\cdot\dfrac{KA_m}{V_l}}{\dfrac{KA_m}{V_l} + \dfrac{1}{T_{1,l}}}\left[1 - \exp\left(\frac{-KA_m}{Q_l} + \frac{-V_l}{T_{1,l}Q_l}\right)\right] \times \exp\left(\frac{-V_f}{2T_{1,f}Q_g} + \frac{-V_{l,t}}{T_{1,l}Q_l}\right) \tag{22}$$

where $1/T_{1,f}$ will lie between the lower limit set by eq 20 and the upper limit set by eq 21, and K is defined in eq 9. Note that the negligible contribution of relaxation within the membrane pores (eq 19) has been omitted for clarity.

4. Results

4.1. NMR Spectroscopy. Figure 2 depicts typical spectra, obtained using the setup shown in Figure 1, to infuse HP ^{129}Xe directly into distilled water. The spectra in Figure 2A,B both display high signal-to-noise ratios (SNRs) and demonstrate the effectiveness of membrane based infusion of concentrated HP ^{129}Xe. Note that high SNR was obtained despite the low coil filling factor used in the experiment (i.e., the 0.13 mL sample volume was ~0.2% that of the coil volume). In Figure 2A, aqueous and gaseous ^{129}Xe peaks are observed because the excess xenon gas from the exchange module was intentionally passed through the RF coil. The spectrum in Figure 2B was

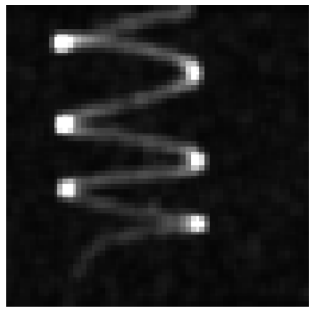

Figure 3. MRI of HP ^{129}Xe dissolved in flowing distilled water (FOV = 4 cm). The HP ^{129}Xe was delivered by the membrane infusion setup shown in Figure 1. The phantom comprised a 1.6 mm ID tube coiled around a 1.5 cm OD cylinder. The image was acquired in less than 9 min with an in-plane resolution of 625 × 625 μm^2.

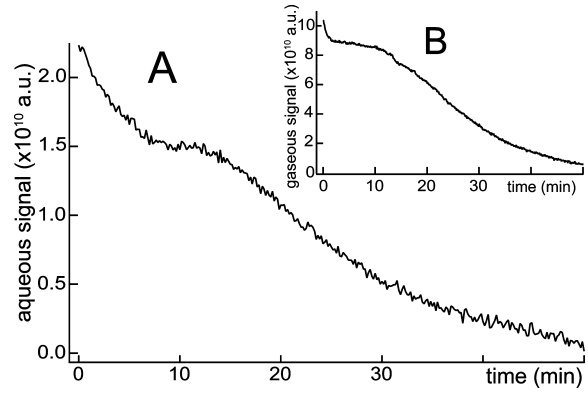

Figure 4. Integrated HP ^{129}Xe signal intensity as a function of time. (A) Dissolved ^{129}Xe signal intensity in distilled water. Three hundred milliliters of HP ^{129}Xe was infused into distilled water using the setup depicted in Figure 1B with gas and liquid flows set to 5 and 20 mL/min, respectively (TR = 5 s). The initial signal intensity was similar to that of the spectrum depicted in Figure 2A. (B) Signal intensity of gas-phase HP ^{129}Xe flowing through the RF coil with the gas exchange module removed (TR = 10 s).

obtained under identical conditions except that excess xenon was exhausted to the outside of the magnet away from the RF coil and, thus, displays no gas-phase ^{129}Xe peak. Further, no gas-phase signal was observed even after averaging 128 scans (data not shown), confirming that membrane-based infusion of HP ^{129}Xe provides high signals without forming xenon gas bubbles.

Figure 2C displays an aqueous ^{129}Xe spectrum obtained by flowing the dilute SEOP (1% xenon) mixture at a total pressure of ~1 atm directly from the polarizer into the exchange module. The spectrum was acquired by averaging signal from 32, 90° RF pulses and employed a sufficiently long repetition time (TR = 5 s) to completely replace the ^{129}Xe magnetization in the sample volume. Despite the full recovery of dissolved ^{129}Xe magnetization, the spectrum displays a substantially lower SNR than do the aqueous peaks shown in Figure 2A,B. This lower SNR occurred even though the polarization of the HP ^{129}Xe flowing directly from the polarizer can be as much as three-times higher than the cryogenically accumulated HP ^{129}Xe.[39] This lower SNR results because the dissolved HP ^{129}Xe concentration is limited by the Ostwald solubility to be at most 10% of the gas-phase xenon concentration,[16] producing a dissolved xenon concentration that is ~100 times lower than can be obtained for concentrated HP ^{129}Xe. Thus, despite the higher polarization of the SEOP mixture, up to a 30-fold lower signal intensity relative to dissolved, cryogenically accumulated ^{129}Xe is expected depending on the duration of the experiment (see Section 4.3).

4.2. MR Imaging of Infused HP ^{129}Xe. The high signal intensities shown in Figure 2A,B suggest that it should be possible to perform rapid MR imaging of dissolved HP ^{129}Xe. Indeed, Figure 3 displays an MR image of HP ^{129}Xe dissolved in water, flowing through a coil of 1.6 mm ID polyethylene tubing that was acquired with an in-plane resolution of 625 × 625 μm^2. The image, which was acquired in less than 9 min, displays an SNR ≈ 10 throughout most of the dissolved ^{129}Xe containing region but also exhibits six brighter regions having SNR ≈ 30. These higher SNR areas correspond to the regions of the phantom where the coiled tubing was perpendicular to the image plane and, thus, contributed a greater volume of xenon-infused water.

4.3. Signal Dynamics from Concentrated HP ^{129}Xe. In some systems, especially biological systems, long-term behavior may be of interest. To assess the ability of infused HP ^{129}Xe to probe these systems, we investigated the HP ^{129}Xe signal intensity as a function of time. As is seen in Figure 4A, the highest signals were observed for about 15 min, but the signal then decayed over the next 35 min. Similar behavior was also observed for initial gas volumes of 100 to 300 mL and gas flows ranging from 2 to 15 mL/min. This signal decay pattern has been reported previously[50] and was attributed to HP ^{129}Xe relaxation within the supply reservoir.

Relaxation in the reservoir should depend on the surface-to-volume ratio within the Tedlar bag and thus be influenced by the initial inflation volume, xenon gas flow, and the duration of the experiment. Gas-phase depolarization within the reservoir is demonstrated in Figure 4B, which shows the gas-phase signal intensity observed by removing the exchange module and passing the HP ^{129}Xe gas at 5 mL/min directly through the RF coil. Other than displaying higher intensity, which is expected from the higher gas-phase xenon concentration, the gas-phase ^{129}Xe signals in Figure 4B exhibit the same general features as the dissolved-phase ^{129}Xe signals shown in Figure 4A.

4.4. Influence of Flow on HP ^{129}Xe Longitudinal Relaxation. The use of exchange membranes limits the time during which HP ^{129}Xe gas contacts the solution of interest. Thus, even though the solutions have not been degassed prior to infusion, the short contact time greatly reduces O_2 induced gas-phase relaxation within the exchange module (see Section 4.6). However, dissolved oxygen may still be a concern, as it has been shown to substantially accelerate the longitudinal relaxation of aqueous ^{129}Xe.[51] To investigate the influence of dissolved O_2, the longitudinal relaxation rate of thoroughly degassed, dissolved ^{129}Xe was compared with the relaxation rate of HP ^{129}Xe that was infused into solution at liquid flows ranging from 4 to 50 mL/min. As seen in Figure 5, the degassed, distilled water yielded an average ^{129}Xe T_1 of 125 s, whereas the average T_1 for the infused HP ^{129}Xe was 92 s. Further the T_1 values for the infused ^{129}Xe varied from ~80 s at the highest liquid flow to ~100 s at the lowest flow. Figure 5 also shows relaxation data from HP ^{129}Xe infused into distilled water at two different xenon gas flows (5 mL/min and 15 mL/min). Although substantial scatter is present, the data suggest that the dissolved ^{129}Xe relaxation rate is relatively insensitive to gas flow.

The sensitivity to liquid flow resulted from the more efficient removal of O_2 from the fluid by the exchange membranes at low liquid flows, which increased the time that the liquid spent within the module. However, the longer T_1 of 100 s suggests that some O_2 must remain in solution after passing through the module. For solutions with stronger relaxation mechanisms than coupling to O_2, the signal intensity dependence on dissolved

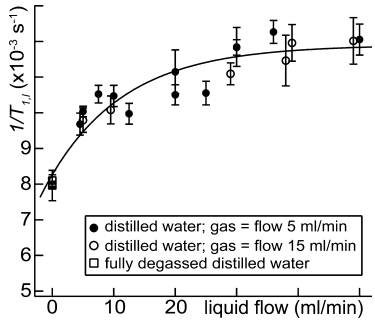

Figure 5. Infused HP ^{129}Xe longitudinal relaxation rate as a function of distilled water flow. The fully degassed data (squares at liquid flow = 0 mL/min) were obtained from dissolved HP ^{129}Xe in a 10 mL plastic syringe. All other data were acquired by temporarily stopping the liquid flow during the measurement. The error bars are statistical errors resulting from the fit. The line is intended as a visual guide only.

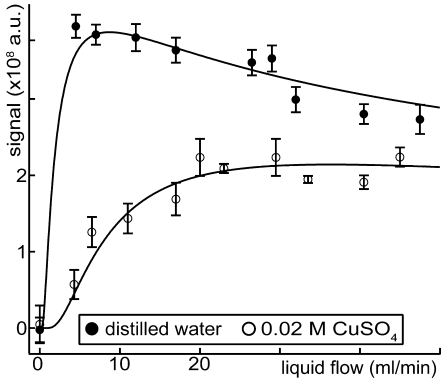

Figure 6. Dissolved HP ^{129}Xe signal as a function of liquid flow. The lines are fits of the data to eq 16, assuming average relaxation times of $T_1 = 92$ s in distilled water and $T_1 = 18$ s in 0.02 M $CuSO_4$. The error bars are the standard deviations from replicate measurements.

oxygen removal is expected to be less pronounced. For instance, in 0.02 M $CuSO_4$, where the ^{129}Xe relaxation should be dominated by paramagnetic Cu^{2+} ions, the average T_1 was only 18 s and ranged from 16.9 to 18.6 s as the liquid flow was varied from 45 to 5 mL/min.

4.5. Liquid Flow Dependent Magnetization Transfer. To validate the model presented in Section 3, the signal from infused HP ^{129}Xe was studied as a function of liquid flow. These experiments were performed using HP gas delivered directly from the polarizer to avoid the complex relaxation behavior exhibited by the concentrated HP ^{129}Xe seen in Figure 4. Although this approach produced a lower dissolved xenon concentration, it simplified data interpretation by providing constant polarization at the gas−liquid interface within the module. The results of these experiments are shown in Figure 6. For distilled water, the signal increased rapidly before reaching a maximum at a liquid flow of ~5 mL/min and then steadily decreased at higher flows. The increasing portion of the curve resulted from higher liquid flows lowering the residence time within the exchange module and the transfer tubing, and, therefore, reducing the polarization lost to relaxation. At higher liquid flows, the signal was reduced because xenon mass transport across the membranes became less efficient.

In a faster relaxing liquid, the signal maximum would be expected to appear at a higher liquid flow and display a lower value. This trend is observed in the signal intensity from the Cu^{2+} doped water, which reaches a maximum value of only about 40% percent of that observed from distilled water. At high enough flows, one would expect the HP ^{129}Xe signal from the Cu^{2+}-containing solution to decrease due to reduced mass transport, but this point lies beyond the operating range of the infusion system used in this work.

Figure 6 also demonstrates the strong quantitative agreement between our empirical results and the theory presented in Sections 3.1 and 3.2. For both aqueous solutions, the data were fit to eq 16 by holding all parameters constant except κ_P, which was used as the sole fitting parameter. The average relaxation times discussed in Section 4.4 were used for $T_{1,l}$ values required for the fittings. All other parameters were held constant at the values provided in Table 1. Despite using literature values from a variety of sources (see Table 1) and average dissolved relaxation times, the κ_P values for the two solutions differed by only 12%, which is within the typical day-to-day variations in polarization.

4.6. Simulating HP ^{129}Xe Infusion. With a detailed understanding of the factors that influence HP ^{129}Xe mass transport and polarization within the membranes, it is possible to evaluate the influence of various experimental parameters on the expected HP ^{129}Xe signal dynamics. Figure 7 shows the results from a series of simulations based on the model presented in Section 3 and summarized in eq 22. Throughout the figure, the observable magnetization, $m_{z,obs}$, is plotted as a fraction of the gas-phase magnetization entering the system, $m_{z,gas}$. Thus the highest possible value would occur at $m_{z,obs}/m_{z,gas} = 0.1068$, which is the Ostwald solubility of xenon water.[16]

Figure 7A displays $m_{z,obs}/m_{z,gas}$ as a function of liquid flow. (Note, gas-phase relaxation has been neglected.) The dotted line depicts $m_{z,obs}/m_{z,gas}$ if longitudinal relaxation is neglected (i.e., only mass transport is considered), and the other two lines represent $m_{z,obs}/m_{z,gas}$ in the presence of two different dissolved ^{129}Xe relaxation times. $T_{1,l} = 125$ s was selected to demonstrate the conditions under which HP ^{129}Xe infusion would be most favorable, and $T_{1,l} = 6$ s was selected as a typical T_1 expected for HP ^{129}Xe in blood.[32] For the mass transport curve, the value of $m_{z,obs}/m_{z,gas}$ approaches the Ostwald solubility limit at the lowest flows but monotonically decreases with increasing liquid flow due to reduced xenon transport. The behavior changes dramatically if the longest dissolved longitudinal relaxation time is considered (solid line) and becomes quite similar to the empirical data for distilled water shown in Figure 6. Similar behavior was also observed for the faster relaxing solution (dashed line). This simulation suggests that little signal intensity would be observed in a fluid with $T_1 = 6$ s under the exact experimental conditions used to produce Figure 6.

Although mass transport into solution depends only weakly upon the gas flow,[37] it is experimentally difficult to quantify the role of gas flow in determining the infused HP ^{129}Xe signal intensity because gas-phase T_1 measurements are complicated by xenon exchange between the gas-phase and the dissolved-phase. Fortunately, as discussed Section 3.3, it is possible to place lower (eq 20) and upper (eq 21) limits on the gas-phase ^{129}Xe longitudinal relaxation rate within the membrane fibers. Figure 7B displays $m_{z,obs}/m_{z,gas}$ as a function of gas flow using both the upper limits on $1/T_{1,f}$. In both limits, $m_{z,obs}/m_{z,gas}$ increases with increasing gas flow but quickly saturates, indicating that only small signal gains are expected at high gas flows. Gas-phase relaxation between the HP ^{129}Xe source and the exchange module is expected to further increase the signal intensity dependence on gas flow. However, we observed no significant advantage in using gas flows that exceeded 5 mL/min.

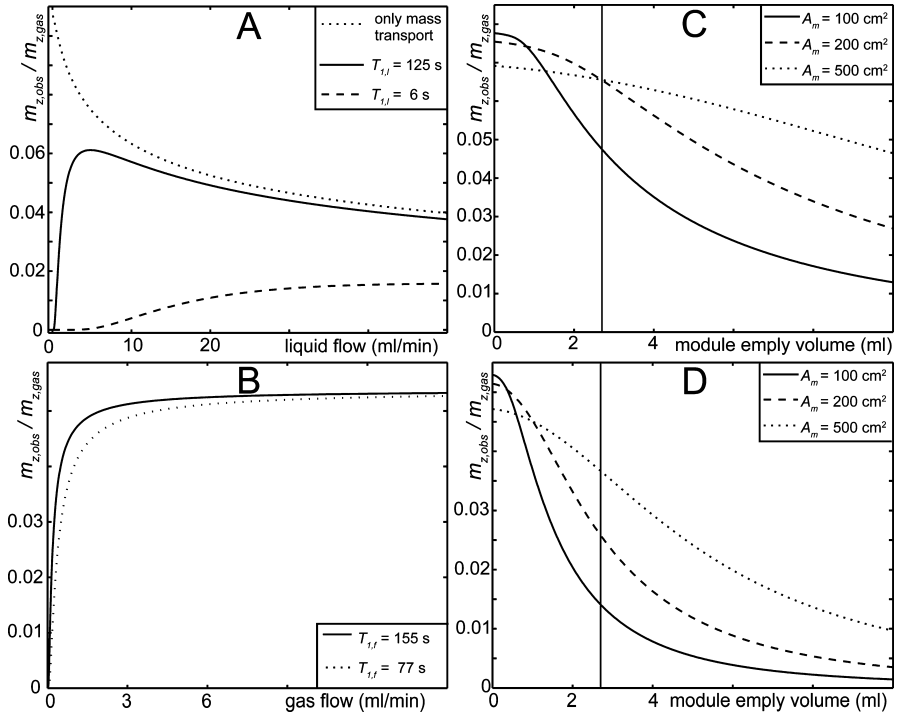

Figure 7. Infusion HP ^{129}Xe magnetization transfer. (A) Observable magnetization relative to the gas-phase magnetization entering the module as a function of liquid flow. The upper curve was produced assuming relaxation was negligible. The two lower curves were produced using the indicated dissolved ^{129}Xe relaxations times. (B) Observable magnetization as a function of gas flow. The two curves correspond to the upper and lower limits on the gas-phase relaxation rates within the module with a liquid flow of 5 mL/min and a dissolved T_1 of 125 s. (C) Observable magnetization as a function of module empty volume at three membrane surface areas. $A_m = 100$ cm^2 matches our experimental conditions. The simulation employed a dissolved T_1 of 125 s and the upper limit on the gas-phase relaxation rate within the module. The vertical line denotes the 2.7 mL empty volume of the exchange module used in the experiments. (D) Same as panel C except the transfer line volume was reduced from 2.26 to 1.0 mL, the liquid flow was increased from 5 to 15 mL/min, and a dissolved T_1 was reduced to 6 s.

Because of relaxation, the optimum HP ^{129}Xe infusion conditions may not be achieved from commercially available exchange models. To evaluate this possibility, we performed a series of simulations in which we assumed the maximum possible gas-phase relaxation (eq 21) while varying the exchange module surface area and empty volume (liquid volume within the exchange module). Figure 7C, which was simulated using a dissolved T_1 of 125 s, indicates that the highest observable magnetization is expected at the lowest empty volumes because dissolved HP ^{129}Xe relaxation within the exchange module is reduced. However, increasing the membrane surface area partially compensates for polarization losses by improving mass transport. For instance, halving the empty volume and doubling the membrane surface area may increase the signal intensity by up to 50%.

The need to optimize magnetization transfer is even more pronounced in quickly relaxing solutions. Figure 7D, which shows the simulated magnetization transfer dynamics at $T_{1,l} =$ 6 s, was produced using identical parameters to those used for Figure 7C except that the transfer line volume was reduced from 2.26 to 1.0 mL and the liquid flow was increased from 5 to 15 mL/min. These changes were made to anticipate the experimental necessities required to work with rapidly relaxing solutions such as blood. These results indicate that the current membrane design is far from optimum for liquids that produce short ^{129}Xe relation times. Fortunately, the advantage expected from reducing the empty volume and increasing the membrane surface area is significantly more pronounced than it is for slowly relaxing liquids. Thus, high dissolved signal intensities should be achievable even in short ^{129}Xe T_1 liquids such as blood.

4.7. Infusing HP ^{129}Xe into Whole Blood. To infuse HP ^{129}Xe into biological fluids, it will be necessary to work with less liquid than is required for the setup shown in Figure 1B. Furthermore, it will be necessary for the membranes to operate for long periods while in contact with complex fluids without fouling or restricting liquid flow. To demonstrate this potential, we replaced the gravity-driven flow setup shown in Figure 1B with a single peristaltic pump. This modification, coupled with reducing the transfer tubing volume to 1.0 mL, allowed us to infuse HP ^{129}Xe into only ~5 mL of whole, heparinized rat blood. A typical spectrum from these experiments is shown in Figure 8 and displays two peaks at 211.6 and 196.9 ppm, which correspond to ^{129}Xe residing in the red blood cells and plasma, respectively. These peak positions are consistent with those observed from in vivo spectroscopy of rats[15] and indicate that interactions with the exchange membranes do not significantly affect the blood.

The spectrum in Figure 8 shows a substantially lower SNR than the spectra in Figure 2A,B, consistent with magnetization losses due to the 4−6 s ^{129}Xe T_1 in blood.[32] While it is difficult to accurately determine the polarization of the ^{129}Xe dissolved in blood, it is possible (using the module empty volume, the liquid transfer volume, $T_1 \sim 6$ s, and a flow of 15 mL/min) to crudely estimate the value at $P \sim 0.5\%$. Fortunately, it is possible to partially compensate for this lower polarization by signal averaging, which could be continued for more than an hour without noticeable membrane module clogging or diminished flow. As a final point, the membranes used with whole blood could be cleaned in accordance with the manufacturer's instructions without noticeably reducing the module performance.

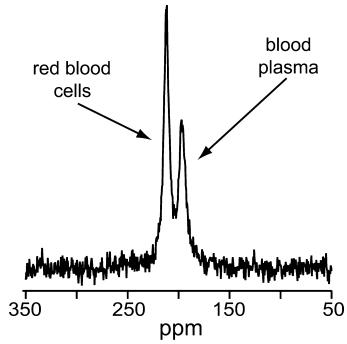

Figure 8. Spectrum of HP ^{129}Xe infused into whole rat blood. The spectrum was acquired by averaging 128 scans (bandwidth = 1.25 kHz, TR = 3 s), and was referenced to gas-phase ^{129}Xe at zero ppm. The peaks at 211.6 and 196.9 ppm correspond to ^{129}Xe in the red blood cells and blood plasma. Blood and xenon flows were set to 15 and 5 mL/min, respectively.

5. Discussion

The experimental setup shown in Figure 1B provides a simple method for producing high aqueous HP ^{129}Xe signal intensities in situations where the volume of the flowing liquid is effectively unlimited, for instance when biomolecules are bound to a matrix such as agarose. For studying samples such as unbound biomolecules or blood, the setup can easily be modified to accommodate much smaller volumes by recirculating the liquid using only a peristaltic pump. Additionally, this second approach is similar to the extracorporeal gas exchange systems currently used in rodent models of cardiopulmonary bypass.[52] This similarity suggests that continuous infusion of HP ^{129}Xe should be suitable for a number of in vivo applications.

By supplying signal continuity, infused HP ^{129}Xe will permit substantial signal averaging and may enable novel studies of fundamental physiological processes in vivo. For instance, when xenon-saturated saline is injected intravenously, the HP ^{129}Xe emerging into the alveolar airspaces provides spatially resolved information about pulmonary perfusion and gas exchange pathways in the lungs.[21] The in vivo availability of injected HP ^{129}Xe, however, is constrained by the tolerable injection volumes. This volume constraint could be eliminated by infusing HP ^{129}Xe directly into the blood using an extracorporeal circuit to enable continuous in vivo delivery of HP ^{129}Xe.[53] Additionally, extracorporeal xenon infusion should also be useful in supplying HP ^{129}Xe to organs other than the lungs.

For these longer duration studies, the influence of the gas-phase relaxation within the HP ^{129}Xe reservoir is a concern. Although the final signal intensity shown in Figure 4A from concentrated xenon is substantially lower than the initial intensity, the SNR observed after 50 min was still as high as that observed in Figure 2C, which was obtained using the dilute (1% xenon) SEOP gas mixture flowing directly from the polarizer. Thus, the higher polarization of the dilute mixture does not offset the higher signal intensity obtained from concentrated HP ^{129}Xe until nearly an hour has elapsed. Because 300 mL batches of concentrated HP ^{129}Xe gas can be readily produced in less than 30 min, cryogenic accumulation is preferable to delivering dilute SEOP mixtures unless the experiment requires constant signal intensity.

Regardless of the gas-phase polarization, it will be advantageous to improve the magnetization transfer into solution. A number of approaches for improving magnetization transfer are suggested by the simulation results. The simplest of these will be to reduce the liquid transfer volumes. Additional gains are expected by optimizing the empty volume and membrane surface area within the exchange module.

6. Conclusions

In this work, we have introduced a method of infusing concentrated HP ^{129}Xe at near ambient pressure directly into flowing solutions using commercially available gas exchange modules. This approach allows the use of hard RF pulses, requires no special sample pretreatment, and avoids potentially problematic bubble formation. By providing large dissolved xenon concentrations, this method yields high HP ^{129}Xe signal intensities and allows dissolved-phase HP ^{129}Xe MR imaging with submillimeter resolution within minutes. Moreover, the infusion of HP ^{129}Xe can be continued, albeit with reductions in signal intensity, for up to an hour using only 300 mL of xenon gas.

We also developed a detailed mathematical model describing the infused HP ^{129}Xe signal dynamics that incorporates gas and fluid flow, mass transport, and longitudinal relaxation. This model suggests that the commercially available modules used in this work do not provide the highest possible ^{129}Xe signal intensities. However, optimized exchange modules should substantially improve aqueous signal intensities.

These modules can also infuse HP ^{129}Xe into complex biological fluids such as blood. More recently, we have successfully used this approach to infuse HP ^{129}Xe into the bloodstream of living rats.[53] This ability to efficiently deliver HP ^{129}Xe to the blood in vivo promises to enable novel studies of the pulmonary system and potentially other organs such as the brain. As a final note, HP ^{129}Xe MR imaging could also be used to visualize and quantify mass transport from the gas-phase into solution and thus provide novel methods for characterizing the gas exchange membranes themselves.

Acknowledgment. The authors wish to thank Bodo von Harten, Horst-Dieter Lemke, and Detlef Krieter from Membrana GmbH for stimulating discussions and supplying some of the gas-exchange modules; Gary P. Cofer for building the ^{129}Xe solenoid probe used in this work; Boma Fubara for assisting with animal preparation; and Sally Zimney for carefully proofreading the manuscript. This work was performed at the Duke Center for In Vivo Microscopy, an NIH/NCRR National Biomedical Technology Research Center (P41 RR005959) and NCI Small Animal Imaging Resource Program (U24 CA092656) with additional support from NHLBI R21 HL087094.

References and Notes

(1) Ratcliffe, C. I. *Annu. Rep. NMR Spectrosc.* **1998**, *36*, 123.
(2) Raftery, D. *Annu. Rep. NMR Spectrosc.* **2006**, *57*, 205.
(3) Ripmeester, J. A.; Ratcliffe, C. I. *J. Chem. Phys.* **1995**, *99*, 619.
(4) Meersmann, T.; Logan, J. W.; Simonutti, R.; Caldarelli, S.; Comotti, A.; Sozzani, P.; Kaiser, L. G.; Pines, A. *J. Phys. Chem. A* **2000**, *104*, 11665.
(5) Smith, M. L.; Dybowski, C. *J. Phys. Chem.* **1991**, *95*, 4942.
(6) Cain, E. J.; Wen, W. Y.; Jost, R. D.; Liu, X.; Dong, Z. P.; Jones, A. A.; Inglefield, P. T. *J. Phys. Chem.* **1990**, *94*, 2128.
(7) Cleveland, Z. I.; Stupic, K. F.; Pavlovskaya, G. E.; Repine, J. E.; Wooten, J. B.; Meersmann, T. *J. Am. Chem. Soc.* **2007**, *129*, 1784.
(8) Goodson, B. M. *J. Magn. Reson.* **2002**, *155*, 157.
(9) Jansch, H. J.; Gerhard, P.; Koch, M. *Proc. Natl. Acad. Sci. U.S.A.* **2004**, *101*, 13715.
(10) Mair, R. W.; Wong, G. P.; Hoffmann, D.; Hürlimann, M. D.; Patz, S.; Schwartz, L. M.; Walsworth, R. L. *Phys. Rev. Lett.* **1999**, *83*, 3324.
(11) Wang, R. P.; Pavlin, T.; Rosen, M. S.; Mair, R. W.; Cory, D. G.; Walsworth, R. L. *Magn. Reson. Imaging* **2005**, *23*, 329.
(12) Anala, S.; Pavlovskaya, G. E.; Pichumani, P.; Dieken, T. J.; Olsen, M. D.; Meersmann, T. *J. Am. Chem. Soc.* **2003**, *125*, 13298.
(13) Ruppert, K.; Brookeman, J. R.; Hagspiel, K. D.; Mugler, J. P. *Magn. Reson. Med.* **2000**, *44*, 349.

(14) Ruppert, K.; Mata, J. F.; Brookeman, J. R.; Hagspiel, K. D.; Mugler, J. P. *Magn. Reson. Med.* **2004**, *51*, 676.
(15) Driehuys, B.; Cofer, G. P.; Pollaro, J.; Mackel, J. B.; Hedlund, L. W.; Johnson, G. A. *Proc. Natl. Acad. Sci. U.S.A.* **2006**, *103*, 18278.
(16) Weathersby, P. K.; Homer, L. D. *Undersea Biomed. Res.* **1980**, *7*, 277.
(17) Lowery, T. J.; Doucleff, M.; Ruiz, E. J.; Rubin, S. M.; Pines, A.; Wemmer, D. E. *Protein Sci.* **2005**, *14*, 848.
(18) Locci, E.; Casu, M.; Saba, G.; Lai, A.; Reisse, J.; Bartik, K. *ChemPhysChem* **2002**, *3*, 812.
(19) Dubois, L.; Da Silva, P.; Landon, C.; Huber, J. G.; Ponchet, M.; Vovelle, F.; Berthault, P.; Desvaux, H. *J. Am. Chem. Soc.* **2004**, *126*, 15738.
(20) Wolber, J.; Cherubini, A.; Leach, M. O.; Bifone, A. *NMR Biomed.* **2000**, *13*, 234.
(21) Driehuys, B.; Möller, H. E.; Cleveland, Z. I.; Pollaro, J.; Hedlund, L. W. *Radiology*, **2009**, *252*, 386.
(22) Swanson, S. D.; Rosen, M. S.; Agranoff, B. W.; Coulter, K. P.; Welsh, R. C.; Chupp, T. E. *Magn. Reson. Med.* **1997**, *38*, 695.
(23) Nakamura, K.; Kondoh, Y.; Wakai, A.; Kershaw, J.; Wright, D.; Kanno, I. *Magn. Reson. Med.* **2005**, *53*, 528.
(24) Spence, M. M.; Rubin, S. M.; Dimitrov, I. E.; Ruiz, E. J.; Wemmer, D. E.; Pines, A.; Yao, S. Q.; Tian, F.; Schultz, P. G. *Proc. Natl. Acad. Sci. U.S.A.* **2001**, *98*, 10654.
(25) Wei, Q.; Seward, G. K.; Hill, P. A.; Patton, B.; Dimitrov, I. E.; Kuzma, N. N.; Dmochowski, I. J. *J. Am. Chem. Soc.* **2006**, *128*, 13274.
(26) Chambers, J. M.; Hill, P. A.; Aaron, J. A.; Han, Z.; Christianson, D. W.; Kuzma, N. N.; Dmochowski, I. J. *J. Am. Chem. Soc.* **2009**, *131*, 563.
(27) Roy, V.; Brotin, T.; Dutasta, J. P.; Charles, M. H.; Delair, T.; Mallet, F.; Huber, G.; Desvaux, H.; Boulard, Y.; Berthault, P. *ChemPhysChem* **2007**, *8*, 2082.
(28) Schroder, L.; Lowery, T. J.; Hilty, C.; Wemmer, D. E.; Pines, A. *Science* **2006**, *314*, 446.
(29) Bifone, A.; Song, Y. Q.; Seydoux, R.; Taylor, R. E.; Goodson, B. M.; Pietrass, T.; Budinger, T. F.; Navon, G.; Pines, A. *Proc. Natl. Acad. Sci. U.S.A.* **1996**, *93*, 12932.
(30) Moller, H. E.; Chawla, M. S.; Chen, X. J.; Driehuys, B.; Hedlund, L. W.; Wheeler, C. T.; Johnson, G. A. *Magn. Reson. Med.* **1999**, *41*, 1058.
(31) Wolber, J.; Cherubini, A.; Leach, M. O.; Bifone, A. *Magn. Reson. Med.* **2000**, *43*, 491.
(32) Wolber, J.; Cherubini, A.; Dzik-Jurasz, A. S. K.; Leach, M. O.; Bifone, A. *Proc. Natl. Acad. Sci. U.S.A.* **1999**, *96*, 3664.
(33) Han, S. I.; Garcia, S.; Lowery, T. J.; Ruiz, E. J.; Seeley, J. A.; Chavez, L.; King, D. S.; Wemmer, D. E.; Pines, A. *Anal. Chem.* **2005**, *77*, 4008.
(34) Driehuys, B.; Cates, G. D.; Miron, E.; Sauer, K.; Walter, D. K.; Happer, W. *Appl. Phys. Lett.* **1996**, *69*, 1668.
(35) Hilty, C.; Lowery, T. J.; Wemmer, D. E.; Pines, A. *Angew. Chem., Int. Ed.* **2006**, *45*, 70.
(36) Baumer, D.; Brunner, E.; Blumler, P.; Zanker, P. P.; Spiess, H. W. *Angew. Chem., Int. Ed.* **2006**, *45*, 7282.
(37) Wickramasinghe, S. R.; Han, B.; Garcia, J. D.; Specht, R. *AIChe J.* **2005**, *51*, 656.
(38) Moller, H. E.; Chen, X. J.; Saam, B.; Hagspiel, K. D.; Johnson, G. A.; Altes, T. A.; de Lange, E. E.; Kauczor, H. U. *Magn. Reson. Med.* **2002**, *47*, 1029.
(39) Driehuys, B.; Pollaro, J.; Cofer, G. P. *Magn. Reson. Med.* **2008**, *60*, 14.
(40) Cates, G. D.; Schaefer, S. R.; Happer, W. *Phy. Rev. A* **1988**, *37*, 2877.
(41) Voorhees, M. E.; Brian, B. F. *Int. Anesthesiol. Clin.* **1996**, *34*, 29.
(42) Wickramasinghe, S. R.; Garcia, J. D.; Han, B. B. *J. Membr. Sci.* **2002**, *208*, 247.
(43) Cussler, E. L. *Mass Transfer in Fluid Systems*, 2nd ed.; Cambridge University Press: New York, 1997.
(44) Matsuda, N.; Sakai, K. *J. Membr. Sci.* **2000**, *170*, 153.
(45) Brodkey, R. S.; Hershey, H. C. *Transport Phenomena: A Unified Approach*; Brodkey Publishing: Columbus, OH, 2003.
(46) Anger, B. C.; Schrank, G.; Schoeck, A.; Butler, K. A.; Solum, M. S.; Pugmire, R. J.; Saam, B. *Phys. Rev. A* **2008**, *78*, 043406.
(47) Deaton, D. M. M.S. Thesis, North Carolina State University, Raleigh, North Carolina, 1998.
(48) Jacob, R. E.; Driehuys, B.; Saam, B. *Chem. Phys. Lett.* **2003**, *370*, 261.
(49) Jameson, C. J.; Jameson, A. K.; Hwang, J. K. *J. Chem. Phys.* **1988**, *89*, 4074.
(50) Moller, H. E.; Chen, X. J.; Chawla, M. S.; Driehuys, B.; Hedlund, L. W.; Johnson, G. A. *J. Magn. Reson.* **1998**, *135*, 133.
(51) Dimitrov, I. E.; Reddy, R.; Leigh, J. S. *J. Magn. Reson.* **2000**, *145*, 302.
(52) Grocott, H. P.; Mackensen, G. B.; Newman, M. F.; Warner, D. S. *Perfusion-UK* **2001**, *16*, 75.
(53) Moller, H. E.; Cleveland, Z. I.; Hedlund, L. W.; Fubara, B.; Cofer, G. P.; Driehuys, B. Proceedings ISMRM 17th Annual Meeting, Honolulu, HI, 2009.
(54) Junker, F.; Veeman, W. S. *Macromolecules* **1998**, *31*, 7010.
(55) Mair, R. W.; Cory, D. G.; Peled, S.; Tseng, C. H.; Patz, S.; Walsworth, R. L. *J. Magn. Reson.* **1998**, *135*, 478.
(56) Wolber, J.; Doran, S. J.; Leach, M. O.; Bifone, A. *Chem. Phys. Lett.* **1998**, *296*, 391.
(57) Yeh, S.; Peterson, R. E. *J. Pharm. Sci.* **1964**, *53*, 822.
(58) *CRC Handbook of Chemistry and Physics*; Lide, D. R., Ed.; CRC Press, LLC: Boca Raton, FL, 2009; Vol. 89.
(59) Butler, J. P.; Mair, R. W.; Hoffmann, D.; Hrovat, M. I.; Rogers, R. A.; Topulos, G. P.; Walsworth, R. L.; Patz, S. *J. Phys.: Condens. Matter* **2002**, *14*, L297.

JP9049582